Table of Contents

- Cover
- Engineering Solutions for CO_2 Conversion
- Copyright
- 1 CO_2 Capture – A Brief Review of Technologies and Its Integration
  - 1.1 Introduction: The Role of Carbon Capture
  - 1.2 CO_2 Capture Technologies
  - 1.3 Integration of Post-combustion CO_2 Capture in the Power Plant and Electricity Grid
  - 1.4 CO_2 Capture in the Industrial Sector
  - 1.5 Conclusions
  - References
  - Notes
- 2 Advancing CCSU Technologies with Computational Fluid Dynamics (CFD): A Look at the Future by Linking CFD and Process Simulations
  - 2.1 Sweep Across the General Simulation Techniques Available
  - 2.2 Multi-scale Approach for CFD Simulation of Amine Scrubbers
  - 2.3 Eulerian, Eulerian–Lagrangian, and Discrete Element Methods for the Simulation of Calcium Looping, Mineral Carbonation, and Adsorption in Other Solid Particulate Materials
  - 2.4 CFD for Oxy-fuel Combustion Technologies: The Application of Single-Phase Reactive Flows and Particle Tracking Algorithms

- 2.5 CFD for Carbon Storage and Enhanced Oil Recovery (EOR): The Link Between Advanced Imaging Techniques and CFD
- 2.6 CFD for Carbon Utilization with Chemical Conversion: The Importance of Numerical Techniques on the Study of New Catalysts
- 2.7 CFD for Biological Utilization: Microalgae Cultivation
- 2.8 What Does the Future Hold?
- References

3 Membranes Technologies for Efficient CO_2 Capture–Conversion

- 3.1 Introduction
- 3.2 Polymer Membranes
- 3.3 Oxygen Transport Membranes for CO2 Valorization
- 3.4 Protonic Membranes
- 3.5 Membranes for Electrochemical Applications
- 3.6 Conclusions and Final Remarks
- References

4 Computational Modeling of Carbon Dioxide Catalytic Conversion

- 4.1 Introduction
- 4.2 General Methods for Theoretical Catalysis Research
- 4.3 Characterizing the Catalyst and Its Interaction with CO2 Using DFT Calculations
- 4.4 Microkinetic Modeling in Heterogeneous Catalysis
- 4.5 New Trends: High-Throughput Screening, Volcano Plots, and Machine Learning

References

5 An Overview of the Transition to a Carbon-Neutral Steel Industry

5.1 Introduction

5.2 Global Relevance of the Steel Industry

5.3 Current Trends in Emission Policies in the World's Leading Countries in Steel Industry

5.4 Transition to a Carbon-Neutral Production. A Big Challenge for the Steel Industry

5.5 CO2 Methanation: An Interesting Opportunity for the Valorization of the Steel Industry Emissions

5.6 Relevant Projects Already Launched for the Valorization of the CO2 Emitted by the Steel Industry

5.7 Concluding Remarks

References

6 Potential Processes for Simultaneous Biogas Upgrading and Carbon Dioxide Utilization

6.1 Introduction

6.2 Overview of Biogas General Characteristics and Upgrading Technologies to Bio-methane Production

6.3 CCU Main Technologies

6.4 Potential Processes for Biogas Upgrading and Carbon Utilization

6.5 Conclusions

References

7 Biogas Sweetening Technologies

7.1 Introduction

7.2 Biogas Purification Technologies

7.3 Biogas Upgrading Technologies

7.4 Conclusions
References
8 CO_2 Conversion to Value-Added Gas-Phase Products: Technology Overview and Catalysts Selection
8.1 Chapter Overview
8.2 CO2 Methanation
8.3 RWGS Reaction
8.4 CO2 Reforming Reactions
8.5 Conclusions and Final Remarks
References
9 CO_2 Utilization Enabled by Microchannel Reactors
9.1 Introduction
9.2 Transport Phenomena and Heat Exchange in Microchannel Reactors
9.3 Application of Microreactors in CO2 Capture, Storage, and Utilization Processes
9.4 Concluding Remarks and Future Perspectives
References
10 Analysis of High-Pressure Conditions in CO_2 Hydrogenation Processes
10.1 Introduction
10.2 Thermodynamic Aspects
10.3 Overview of Some Industrial Approaches Focused on the Production of Valuable Compounds form CO2 Using a Carbon Capture and Utilization (CCU) Approach
10.4 Techno-Economic Considerations for the Methanol Production from a CCU Approach with the Use of High Pressure
10.5 Concluding Remarks

- References
- Notes

11 Sabatier-Based Direct Synthesis of Methane and Methanol Using CO_2 from Industrial Gas Mixtures

- 11.1 Overview
- 11.2 Methane Synthesis of Gas Mixtures
- 11.3 Applications
- 11.4 Methanol Synthesis
- Acknowledgments
- References

12 Survey of Heterogeneous Catalysts for the CO_2 Reduction to CO via Reverse Water Gas Shift

- 12.1 Introduction
- 12.2 RWGS Catalysts
- 12.3 Mechanism of RWGS Reaction
- References

13 Electrocatalytic Conversion of CO_2 to Syngas

- 13.1 Introduction
- 13.2 Production of Syngas
- 13.3 Electroreduction of CO2/Water Mixtures to Syngas
- 13.4 Conclusions
- Acknowledgments
- References

14 Recent Progress on Catalyst Development for CO_2 Conversion into Value-Added Chemicals by Photo- and Electroreduction

- 14.1 Introduction
- 14.2 CO2 Catalytic Conversion by Photoreduction

  14.3 CO_2 Catalytic Conversion by Electroreduction
  References
15 Yolk@Shell Materials for CO_2 Conversion: Chemical and Photochemical Applications
  15.1 Overview
  15.2 Key Benefits of Hierarchical Morphology
  15.3 Materials for Chemical CO2 Recycling Reactions
  15.4 Synthesis Techniques for CS/YS: A Brief Overview
  15.5 Future Advancement
  References
16 Aliphatic Polycarbonates Derived from Epoxides and CO_2
  16.1 Introduction
  16.2 Aliphatic Polycarbonates
  16.3 Catalyst Systems for the CO2/Epoxide Copolymerization
  16.4 Conclusion
  References
17 Metal–Organic Frameworks (MOFs) for CO_2 Cycloaddition Reactions
  17.1 Introduction to MOF
  17.2 MOFs as Catalysts
  17.3 CO_2 Cycloadditions
  17.4 Oxidative Carboxylation
  References
18 Plasma-Assisted Conversion of CO_2
  18.1 Introduction

18.2 Plasma-catalytic CO2 Conversion
18.3 Perspective
18.4 Conclusion
References
Index
End User License Agreement

List of Tables

Chapter 1

Table 1.1 Advantages of each type of membrane [21].
Table 1.2 Desired solvent properties and its impact on the absorption process...
Table 1.3Low heat value (LHV) efficiency, carbon intensity, and energy penalty i...

Chapter 2

Table 2.1 Summary of published CFD studies concerning amine scrubbers.
Table 2.2 Summary of published CFD studies concerning carbon capture technolo...
Table 2.3 Summary of published CFD studies concerning oxy-fuel technologies.

Chapter 3

Table 3.1 Hydrogen-selective membrane types [70, 71].
Table 3.2 Summary of main characteristics of electrolyzers [103–105].

Table 3.3 Summary of main features of CO electrolyzers or co-electrolyzers.

Chapter 6

Table 6.1 Biogas composition from different sources [13,15,18–22].

Table 6.2 Technical features of biogas upgrading technologies.

Table 6.3 Energy consumption and efficiency range of biogas upgrading technol...

Table 6.4 Precipitation with Ca$^{\pm}$–Mg$^{\pm}$-rich compound studies.

Chapter 7

Table 7.1 Contaminant treatability for the major purification technologies [2...

Table 7.2 Advantages and disadvantages of techniques for removal of water [16...

Chapter 10

Table 10.1 Gibbs free energy, enthalpy change, and standard equilibrium const...

Table 10.2 Companies and institutions involved in the production of methanol ...

Table 10.3 PtG (demonstration) projects in Europe reported by the European Po...

Table 10.4 Mass and energy balance for the methanol CCU plant according to bi...

Table 10.5 Economic evaluation for the methanol CCU plant according to biblio...

Table 10.6 Environmental evaluation for the methanol CCU plant according to b...

Chapter 11

Table 11.1 Overview of the catalysts employed in the methanation studies.

Table 11.2 Overview of the CO_2 content of some gas mixtures in industrial app...

Table 11.3 Composition of oxyfuel and conventional flue gas from lignite powe...

Chapter 12

Table 12.1 Selection of some recent work in CO_2 hydrogenation to CO.

Chapter 13

Table 13.1 Summary of some of the most relevant studies dealing with the prod...

Chapter 17

Table 17.1 List of different MOFs and their performance in cycloaddition reac...

List of Illustrations

Chapter 1

Figure 1.1 Diagram of pre-combustion capture for power generation in IGCC....

Figure 1.2 Process schematic of a simplified commercial scale natural gas Al...

Figure 1.3 The adsorption process: (a) difference of physisorption and chemi...

Figure 1.4 Comparison of TSA and PSA for the regeneration of solid adsorbent...

Figure 1.5 Calcium looping system as post-combustion configuration.

Figure 1.6 Chemical looping combustion. Me_xO_y/Me_xO_{y-1} denotes the reci...

Figure 1.7 Scheme of a single-stage membrane system.

Figure 1.8 General chemical absorption configuration

Figure 1.9 Two main options for CO_2 capture using fuel cells. (a) The FC oxi...

Figure 1.10 Superstructure of SOFC – CO_2 capture process configurations.

Figure 1.11 Schematic integration of a power plant with a post-combustion CO

Figure 1.12 Review of current TRL of different CO_2 capture technologies. *Th...

Chapter 2

Figure 2.1 Time and length scales of the simulation methods available for CC...

Figure 2.2 This schematic illustration depicts the flow of information betwe...

Figure 2.3 (a) Details of the space discretization of the calciner, (b) map ...

Figure 2.4 (a) Details of the volume fraction map describing the liquid flow...

Figure 2.5 (a) Parity plot showing the match between the numerical and the e...

Figure 2.6 Pressure maps within PBR reactors obtained using CFD simulations ...

Chapter 3

Figure 3.1 Gas transport through a membrane.

Figure 3.2 Diffusion and solubility coefficient for different polyimides....

Figure 3.3 Upper bound correlation for (a) CO_2/CH_4 separation and (b) CO_2/N_2

Figure 3.4 (a, b) Steps involved in the oxygen permeation through an oxygen ...

Figure 3.5 Simplified process layouts for oxygen permeating membrane modules...

Figure 3.6 Enthalpy and free energy of CO_2 and H_2O reduction reactions and w...

Figure 3.7 Schematic representation of the CO_2 and Co-electrolyzer systems....

Figure 3.8 (a) Representation of the four chemical steps. (b) Protonic membr...

Figure 3.9 Co-ionic catalytic membrane reactor.

Chapter 4

Figure 4.1 Overview of reaction pathways for CO_2 toward different products. ...

Figure 4.2 Reaction path for methanol synthesis (MS) by CO_2 hydrogenation on...

Figure 4.3 Proposed mechanism for dry reforming of methane on Ni catalyst....

Figure 4.4 (a) 2D contour map of the theoretical reduction potential in term...

Figure 4.5 Cartoon of the neural network potential used to directly relax an...

Chapter 5

Figure 5.1 World crude steel production in million tonnes reported by the Wo...

Figure 5.2 Regional share of steel production in 2018.

Figure 5.3 Stainless steel market diagram adapted from that published by the...

Figure 5.4 Main actors and actions for the transition toward a zero-emission...

Figure 5.5 Power-to-X concepts overview.

Chapter 6

Figure 6.1 Annual record of CO_2 concentration in the atmosphere from 2013 to...

Figure 6.2 Evolution of biogas production plants from 2010 to 2016.

Figure 6.3 Some options for bio-methane use after upgrading process.

Figure 6.4 Main CCU technologies.

Figure 6.5 Options for coupling biogas upgrading and CCU.

Figure 6.6 CO_2 capture from biogas and utilization in drink–food industry or...

Figure 6.7 CO_2 capture from biogas and precipitation with Ca^{2+}–Mg^{2+}-...

Figure 6.8 Membrane plus CO_2 storage for food application.

Figure 6.9 Biogas upgrading through membrane separation and methanation.

Figure 6.10 Biogas upgrading via cryogenic methods and dry ice production.

Figure 6.11 Biogas upgrading via cryogenic methods and supercritical CO_2 pro...

Chapter 7

Figure 7.1 Biological filters: (a) bioscrubber, (b) biofilter, and (c) biotr...

Figure 7.2 The chemical structure of three typical siloxanes.

Figure 7.3 Typical unit operations for the upgrading of biogas.

Figure 7.4 Schematic representation of a typical water scrubbing system.

Figure 7.5 Schematic representation of a typical water organic solvent scrub...

Figure 7.6 Schematic representation of a typical chemical (amine) scrubbing ...

Figure 7.7 Schematic representation of a typical pressure swing adsorption (...

Figure 7.8 Schematic representation and operational principle of a tubular h...

Figure 7.9 Schematic representation of a simple membrane upgrading system.

Figure 7.10 Three alternative designs of membrane stages: (a) without biogas...

Figure 7.11 Schematic representation of a simple three-stage cryogenic bioga...

Chapter 8

Figure 8.1 Concept for the storage of renewable energy in gas distribution s...

Figure 8.2 Schematic of the intensified reverse water-gas shift-chemical loo...

Figure 8.3 Flow sheet of a reforming process with optional configurations (d...

Figure 8.4 TEM images of (a) CeO_2-NRs, (b) CeO_2-NCs, and (c) CeO_2-NPs; high-...

Chapter 9

Figure 9.1 Some benefits of process intensification.

Figure 9.2 Heat and mass transfer performance of various types of reactors....

Figure 9.3 (a) Schematic representation of characteristic regimes observed i...

Figure 9.4 Heat transfer characteristic data: (a) Illustrative representatio...

Figure 9.5 (a) Schematic representation of the microchannel reactor includin...

Figure 9.6 An overall schematic representation of the utilization of microch...

Figure 9.7 (a) Representation of a single microchannel with a deposited cata...

Figure 9.8 Schematic representation of in situ CH_4/O_2 production as a propel...

Figure 9.9 Overview of the transformation routes of CO_2 into C_{2+} chemica...

Scheme 9.1 Reaction of CO_2 cycloaddition with epoxides.

Chapter 10

Figure 10.1 Bulk chemicals based in CO_2 hydrogenation reactions. Products wi...

Figure 10.2 Renewable methanol production using renewable hydrogen and waste...

Figure 10.3 Proposed CCU methanol plant for the techno-economic evaluation....

Figure 10.4 Strategy for the techno-economic analysis.

Figure 10.5 Evaluation of variable annual cost (M€ yr^{-1}) and methanol ...

Figure 10.6 Evaluation of payback period (PBP) and benefit–cost ratio (BCR) ...

Chapter 11

Figure 11.1 Calculation of the temperature and pressure dependency of the co...

Figure 11.2 Schematic illustration of the setup for the direct methanation. ...

Figure 11.3 Performance as a function of the content of oxygen in synthetic ...

Figure 11.4 Synthetic flue gas: temperature and CO_2 conversion versus conten...

Figure 11.5 Catalytic performance versus time. CO_2 with 516 ppm SO_2 is used....

Figure 11.6 (a) Conversion of CO (empty circles) and CO_2 (black circles) ver...

Figure 11.7 Diagram for an oxyfuel CO_2 circuit for an energy supply system w...

Figure 11.8 Demand of gas flow of the Wankel engine, stable at 50 Hz, with r...

Figure 11.9 Sketch of an integrated system applying electrolysis, direct flu...

Figure 11.10 Setup of our high-pressure methanol reactor with an integrated ...

Figure 11.11 (a) The influence of N_2 on the CO_2 conversion rate (left scale)...

Chapter 12

Figure 12.1 CO_2 conversion as a function of temperature over (1) Au/CeO_2 cat...

Figure 12.2 Dependence of CO_2 conversion on temperature for Au/TiO_2, TiO_2, a...

Figure 12.3 Catalytic performance of Au/TiO_2 and Au/Al_2O_3 catalysts in RWGS ...

Figure 12.4 Arrhenius plots for the Au/TiO_2 and Au/Al_2O_3 catalysts in RWGS r...

Figure 12.5 (a) CO_2 conversion and (b) CO selectivity as a function of react...

Figure 12.6 Effect of reduction and oxygen pretreatment of Ru/CeO_2 catalyst ...

Figure 12.7 CO formation rate per catalyst weight and activation energy as a...

Figure 12.8 Stability of 1 wt% Cu/β-Mo_2C catalyst and the commercial 36 wt% ...

Figure 12.9 CO selectivity and CH_4 selectivity for Fe/Al_2O_3, Fe–Cu/Al_2O_3, Fe...

Figure 12.10 Comparison of CO and CH_4 selectivity on 0.5% and 10% Ni/SiO_2 ca...

Figure 12.11 Relative activity of Ni/CeO_2, Fe/CeO_2, and Fe-incorporated Ni/C...

Figure 12.12 Stable CO_2 conversion was obtained over 3 wt% Ni/Ce–Zr–Ox catal...

Figure 12.13 Proposed reaction mechanism of the RWGS reaction over Pt/CeO_2 c...

Chapter 13

Figure 13.1 Number of scientific publications containing the topic *“electroc...*

Figure 13.2 Scheme of a typical membrane electrode assembly used to carry ou...

Figure 13.3 Scheme of a bipolar membrane-based electrochemical cell used for...

Figure 13.4 Scheme of the electrocatalyst developed by Cho and coworkers to ...

Figure 13.5 Effect of the CO_2 concentration on the reaction rates of (a) CO_2

Chapter 14

Figure 14.1 A schematic view of solar-driven CO_2-to-fuel strategy; a two-ste...

Figure 14.2 Schematic diagram showing the photocatalytic process for H_2 prod...

Figure 14.3 Tuning the selectivity of solar-driven CO_2 hydrogenation over Co...

Figure 14.4 An overall schematic presentation of the sustainable energy econ...

Figure 14.5 Proposed reaction pathway for CO_2 electrocatalytic reduction on ...

Figure 14.6 Schematic illustration depicts the several advantages of ultrath...

Chapter 15

Figure 15.1 Graphic representation of core–shell and yolk–shell particles.

Figure 15.2 (a) Publication metrics for papers published concerning sinterin...

Figure 15.3 Volcano plot displaying the activity against binding energies of...

Figure 15.4 Demonstration of the established equilibrium distance ($d_{M–S}$...

Figure 15.5 Diagram of the conduction band (white squares) and valence band ...

Figure 15.6 Diagram of how light interacts and refracts with solid, hollow, ...

Figure 15.7 Schematic illustration of several YS variations: (a) standard si...

Figure 15.8 Schematic illustration of how soft templating can achieve either...

Chapter 16

Figure 16.1 Alternating copolymerization of CO_2 with (a) propylene oxide, (b...

Figure 16.2 Oxidation of (*R*)-limonene via two different routes to diff...

Scheme 16.1 Copolymerization of CO_2 and epoxides in three elementary steps: ...

Figure 16.3 Reaction coordinate diagram for the coupling of (a) CHO and (b) ...

Scheme 16.2 Degradation mechanism for PPC: chain scission (a) and backbiting...

Figure 16.4 Poly(cyclohexene carbonate) (a), poly(propylene carbonate) (b), ...

Figure 16.5 Representation of part of the repeating unit in two different zi...

Figure 16.6 Types of homogeneous catalysts active in the copolymerization of...

Scheme 16.3 Proposed copolymerization mechanism for BDI–Zn catalysts (a) and...

Figure 16.7 Flexibly tethered bimetallic zinc complex.

Figure 16.8 Structure of the β-diiminato–zinc–$NTMS_2$ complex **3** and its ORTEP ...

Figure 16.9 Macrocyclic diphenolate complexes with Zn or Mg as a central met...

Figure 16.10 Postulated mechanism for the terpolymerization reaction of BBL,...

Figure 16.11 Active initiators for the copolymerization of CO_2 and limonene ...

Figure 16.12 Postulated mechanism for the copolymerization of limonene oxide...

Chapter 17

Figure 17.1 Schematic representation of the MOF structural levels and compon...

Figure 17.2 Examples of different applications involving MOF materials.

Figure 17.3 Generation of open metal site (OMS) illustrative example.

Scheme 17.1 Synthesis of cyclic carbonates from an epoxide.

Figure 17.4 Proposed mechanism of CO_2 cycloaddition.

Scheme 17.2 Oxidative carboxylation reaction of styrene.

Chapter 18

Figure 18.1 Energy efficiency of plasma-assisted CO_2 reduction as a function...

Figure 18.2 Illustration of different electron impact driven dissociation pr...

Figure 18.3 Channels for activation of CO_2 as a function of the reduced elec...

Figure 18.4 Various plasma reactors used for chemical conversions: dielectri...

Figure 18.5 Schematic representation of various plasma–catalyst interactions...

Figure 18.6 Schematic of the dissociative surface adsorption of various acti...

Figure 18.7 Comparison of literature data for CO_2 splitting in various plasm...

Figure 18.8 Comparison of literature data for the dry reforming of methane i...

Figure 18.9 Comparison of literature data for CO_2 hydrogenation in various p...

Figure 18.10 Comparison of literature data for artificial photosynthesis in ...

Figure 18.11 Typical timescales of plasma-phase reactions and catalytic surf...

Figure 18.12 Industrial plasma-driven ozone generators (DBD reactors) for 60...

Engineering Solutions for CO_2 Conversion

Edited by

Tomas R. Reina
José A. Odriozola
Harvey Arellano-Garcia

WILEY-VCH

Editors

Dr. Tomas R. Reina
University of Surrey
Department of Chemical & Process Engineering
388 Stag Hill
GU2 7XH Guildford, Surrey
United Kingdom

Prof. José A. Odriozola
Universidad of Sevilla
Inorganic Chemistry Department
4 San Fernando Street
41004 Sevilla
Spain

Prof. Harvey Arellano-Garcia
University of Surrey
Department of Chemical & Process Engineering
388 Stag Hill
GU2 7XH Guildford, Surrey
United Kingdom

Cover Image: © cozyta/Getty Images

All books published by **Wiley-VCH** are carefully produced. Nevertheless, authors, editors, and publisher do not warrant the information contained in these books, including this book, to be free of errors. Readers are advised to keep in mind that statements, data, illustrations, procedural details or other items may inadvertently be inaccurate.

Library of Congress Card No.:
applied for

British Library Cataloguing-in-Publication Data
A catalogue record for this book is available from the British Library.

Bibliographic information published by
the Deutsche Nationalbibliothek
The Deutsche Nationalbibliothek lists this publication in the Deutsche Nationalbibliografie; detailed bibliographic data are available on the Internet at <http://dnb.d-nb.de>.

© 2021 WILEY-VCH GmbH, Boschstr. 12, 69469 Weinheim, Germany

All rights reserved (including those of translation into other languages). No part of this book may be reproduced in any form – by photoprinting, microfilm, or any other means – nor transmitted or translated into a machine language without written permission from the publishers. Registered names, trademarks, etc. used in this book, even when not specifically marked as such, are not to be considered unprotected by law.

Print ISBN: 978-3-527-34639-4

ePDF ISBN: 978-3-527-34650-9

ePub ISBN: 978-3-527-34651-6

oBook ISBN: 978-3-527-34652-3

1

CO_2 Capture – A Brief Review of Technologies and Its Integration

Mónica García[1], Theo Chronopoulos[2], and Rubén M. Montañés[3]

[1]International Energy Agency- Greenhouse Gas R&D Programme (IEAGHG), Pure Offices, Hatherley Lane, Cheltenham, GL51 6SH, United Kingdom

[2]128/15 Hoxton Street, N1 6SH, London, United Kingdom

[3]Energy Technology, Chalmers University of Technology, Department of Space, Earth and Environment, Hörsalsvägen 7B, SE-412 96, Gothenburg, Sweden

1.1 Introduction: The Role of Carbon Capture

The Intergovernmental Panel for Climate Change (IPCC) recently released the special report on 1.5C [1] and pointed out the need to implement all available tools to cut down CO_2 emissions. Energy efficiency, fuel switching, renewables, and carbon capture represent the largest impact on CO_2 emission reduction in power and industrial sectors. Carbon capture represents a contribution of 23% in the “Beyond 2 degrees scenario” (B2DS) modeled by the International Energy Agency (IEA)[1] and has other interesting characteristics that increase its value beyond its cost: (i) easiness to retrofit current power plants or industrial facilities,[2] (ii) simplicity to integrate that in the electricity grid and offer an interesting tool to cover the intermittency of renewables, (iii) ideal to cut down industrial process emissions that otherwise cannot suffer deep reductions, and (iv) current carbon budgets rely on negative emissions to compensate the use of fossil fuels [1]. Carbon capture combined with bioenergy (BECCS) can provide negative emissions at large scale in an immediate future.

CO_2 capture (also called CO_2 sequestration or carbon capture) involves a group of technologies aiming to separate CO_2 from other compounds released during the production of energy or industrial products, obtaining a CO_2-rich gas that can be stored or used for the obtention of valuable products. The main classification of CO_2 capture technologies relies on where in the process the CO_2 separation occurs. For the power sector, it can be divided into pre-, oxy-, and post-combustion. For the industrial sector, the classification is similar, although their integration would be different. In addition, other new arrangements are emerging.

1.2 CO_2 Capture Technologies

1.2.1 Status of CO_2 Capture Deployment

GCCSI reported in 2018 23 large-scale CCS facilities in operation or under construction globally, summing up 37 $MtCO_2$ per year. This wide range of facilities shows the versatility of CO_2 capture processes.[3]

In the power sector, the United States is leading the implementation deployment, although Europe has the highest CO_2 capture capacity. The Boundary Dam project (Canada) and Petra Nova (USA) are pioneers in reaching commercial scale. Moreover, based on the successful results of the Boundary Dam project, a CO_2 capture facility has been planned for the Shand power facility (Canada), incorporating not only learnings from the Boundary Dam but also enhanced thermal integration and tailored design. The results show a significant cost reduction [2]. Also in Canada, the Quest project completes the list of Canadian CCS projects in operation [3] and The National Energy Laboratory (NET) power project recently appeared in the United States as a potential significant reduction on CO_2 capture costs [4].

In the industrial sector, cement, steel, refining, chemicals, heavy oil, hydrogen, waste-to-energy, fertilizers, and natural gas have been identified by the Carbon Sequestration Leadership Forum (CSLF; https://www.cslforum.org) as the main intensive emitter industries. As it is highlighted, the Norcem Brevik plant [5, 6], LEILAC [7] (cement production), and Al Redayah (steel production) are on the way to start running carbon capture systems in industrial facilities at pilot and large scales.

1.2.2 Pre-combustion

Pre-combustion systems can be applied to natural gas combined cycles (NGCC) or integrated gasification combined cycle (IGCC) (Figure 1.1), where a syngas, comprising mainly CO and H_2, feeds a gas turbine (GT) combined cycle system to produce electricity. The potential advantages are higher conversion efficiencies of coal to electricity and cheaper removal of pollutants [8]. The syngas, based on the water shift reaction, can be converted into CO_2 and H_2O. This mixture is typically separated with physical solvents (as described in Section 1.2.4), membranes, or sorbents. However, hybrid technologies can also be used. Depending on the technology, further post-treatment would be needed to avoid degradation and loss of efficiency.

The main theoretical advantage of pre-combustion is the production of hydrogen, which will add value to the business model, and a lower energy penalty compared to using the traditional chemical absorption within a post-combustion configuration. However, large projects demonstrated that this difference is only 1–2%, as reported by National Energy Technology Laboratory (NETL) [9].

The most notable pre-combustion project was the Kemper County IGCC plant in the United States, which stopped its operation in 2017.This demonstration facility would place this arrangement at high TRL, while other testing campaigns would reach up to a TRL of 6.

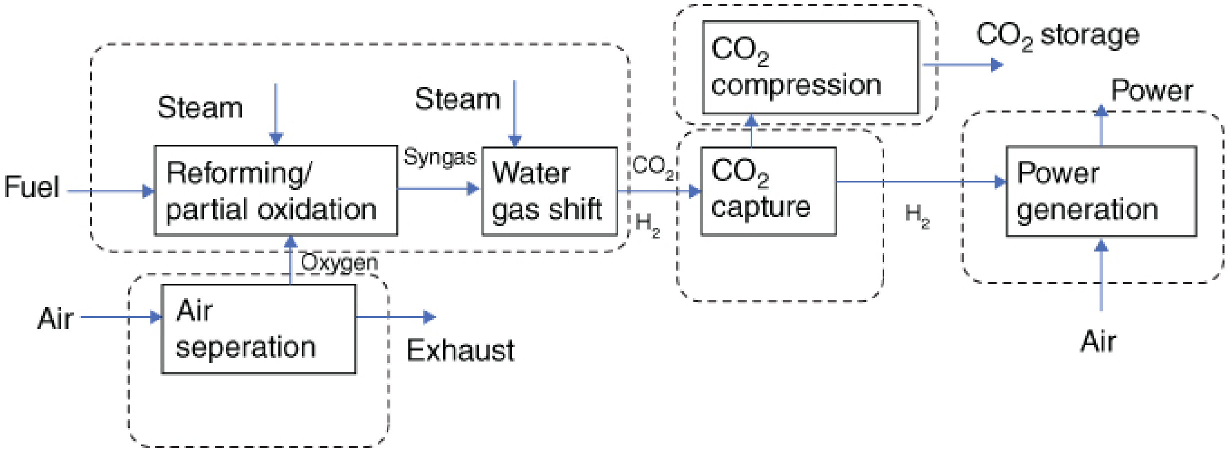

Figure 1.1 Diagram of pre-combustion capture for power generation in IGCC.

Source: Adapted from Jansen et al. [72].

1.2.3 Oxyfuel

In the oxyfuel process, the air is split into nitrogen and oxygen, generally using an air separation unit (ASU), for the combustion of fuel with nearly pure oxygen. The consequence is a higher flame temperature and a highly concentrated CO_2 stream (60–75%, wet and might contain impurities and incondensable components) that can be further purified to meet the final use specifications. The

CO_2-rich gas is typically recirculated to manage the unstable flame and its high temperature. Nowadays, the progress on oxyfuel combustion is focused on the reduction of air separation costs and the enhancement of process configuration to reduce capture costs. Further information can be found, for example, in Ref. [10]. Based on the current progress, the most advanced arrangements can be assessed as TRL 7.

An advanced oxyfuel process, called the Allam cycle (Figure 1.2), is being tested at large scale as part of the NET Power project in the United States [4]. This involves oxyfuel combustion and a high-pressure supercritical CO_2 working fluid in a highly recuperated Brayton cycle, aiming to reduce CO_2 capture costs and prove stable operation. Based on that, there is a potential to progress to a TRL of 7 once the facility is fully operational.

1.2.4 Post-combustion

Post-combustion refers to the group of technologies able to separate CO_2 from the flue gas emitted during the fuel combustion and/or other reactions in the industrial sector. This indicates that those systems are mainly installed as additional equipment downstream in new plants or during the retrofitting of the existing facilities. The latter represents the main advantage of post-combustion technologies compared to pre- or oxy-combustion, as a fundamental redesign or complex integration with the existing facilities would be minimal.

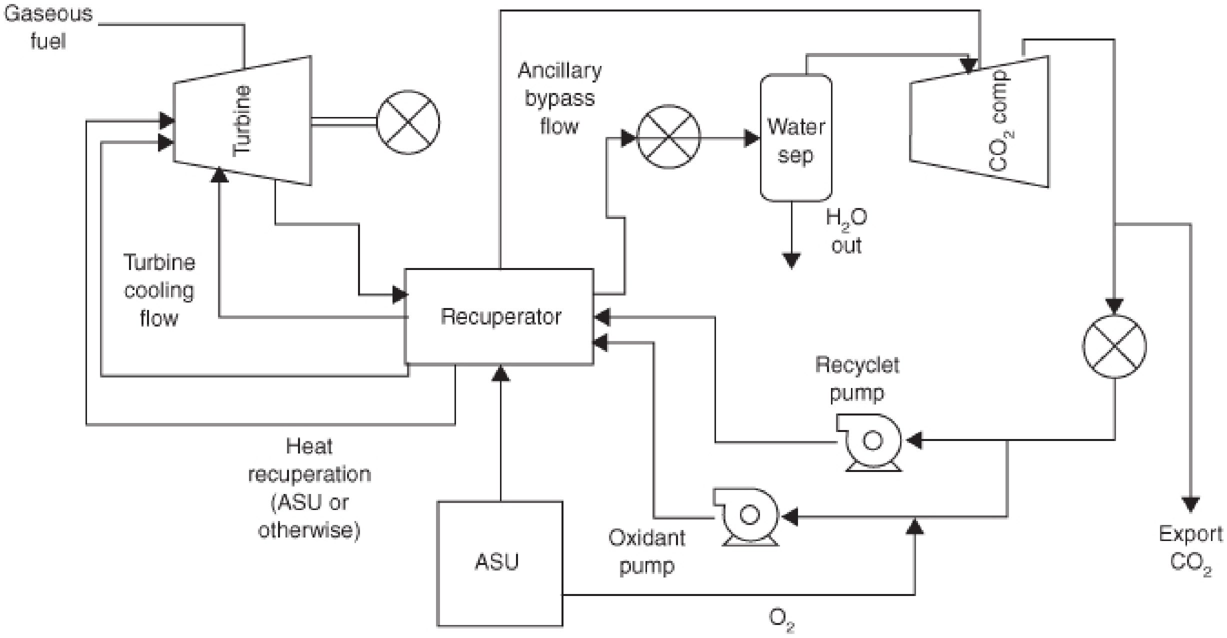

Figure 1.2 Process schematic of a simplified commercial scale natural gas Allam cycle.

Source: Adapted from Allam et al. [4].

1.2.4.1 Adsorption

Adsorption refers to the uptake of CO_2 molecules onto the surface of another material. Based on the nature of interactions, adsorption can be classified into two types: (i) physical adsorption and (ii) chemical adsorption. In physical adsorption, the molecules are physisorbed because of physical forces (dipole–dipole, electrostatic, apolar, hydrophobic associations, or van der Waals) and the bond energy is 8–41 kcal mol^{-1}, while in chemical adsorption, the molecules are chemisorbed (chemical bond; covalent, ionic, or metallic) and the bond energy is about 60–418 kcal mol^{-1} [11].

A theoretical advantage of adsorption against other processes is that the regeneration energy should be lower compared to absorption because the heat capacity of a solid sorbent is lower than that of aqueous solvents. However, other parameters, such as working capacity and